Research Article

Henrik Lietz*, M. Muneeb Hassan and Jörg Eberhardt

Optical lens-shift design for increasing spatial resolution of 3D ToF cameras

DOI 10.1515/aot-2016-0063
Received December 1, 2016; accepted December 22, 2016; previously published online January 25, 2017

Abstract: Sensor resolution of 3D time-of-flight (ToF) outdoor-capable cameras is strongly limited because of its large pixel dimensions. Computational imaging permits enhancement of the optical system's resolving power without changing physical sensor properties. Super-resolution (SR) algorithms superimpose several sub-pixel-shifted low-resolution (LR) images to overcome the system's limited spatial sampling rate. In this paper, we propose a novel opto-mechanical system to implement sub-pixel shifts by moving an optical lens. This method is more flexible in terms of implementing SR techniques than current sensor-shift approaches. In addition, we describe a SR observation model that has been optimized for the use of LR 3D ToF cameras. A state-of-the-art iteratively reweighted minimization algorithm executes the SR process. It is proven that our method achieves nearly the same resolution increase as if the pixel area would be halved physically. Resolution enhancement is measured objectively for amplitude images of a static object scene.

Keywords: 3D ToF photonic mixing device (PMD) camera; lens-shift design; multiframe image processing; super-resolution; three-dimensional imaging.

1 Introduction

Fast and robust reconstruction of objects in three dimensions is highly demanded. Not only autonomous systems like robots and vehicles but also production lines in industrial manufacturing or multimedia applications in consumer electronics require additional information in the third dimension. Time-of-flight (ToF) cameras benefit fast and robust three-dimensional (3D) data acquisition in real time by measuring the running time of an emitted signal for each pixel at the same time [1]. However, a considerable limitation is their low sensor resolution resulting in loss of detail at further distances. Reducing pixel size physically decreases its sensitivity and, consequently, the accuracy and distance range of a ToF system. Computational imaging permits resolution-enhancing techniques without changing the physical sensor properties such as pixel and sensor size. Super-resolution (SR) superimposes several sub-pixel-shifted low-resolution (LR) images to increase spatial resolution significantly [2–4]. Shifting the image sensor is an intuitive way of implementing sub-pixel shifts [5]. Adversely, the room for actuators has to be considered from the very beginning of designing the camera. The major focus of this paper is the introduction of a new approach that allows subsequent implementation of SR for nearly every type of digital camera by redesigning the imaging optics. Our method shifts a lens to force a sub-pixel shift on the image plane of a large pixel photonic mixing device (PMD) sensor. We then use a state-of-the-art iteratively reweighted SR algorithm [6] to reconstruct high-resolution amplitude and distance images. SR results are evaluated by the slanted edge method [7, 8] to determine the system's real optical resolving power. Evaluation is focused on amplitude images as this image type can be used for classical object recognition applications and profits most of resolution enhancement. Our proposed lens-shift approach is compared with a conventional sensor-shift method. Gradient edge descent method determines spatial resolution enhancement in both amplitude and distance image.

2 Related work

PMD cameras belong to ToF systems as they measure the running time of an inherent signal by periodically emitting amplitude-modulated near-infrared (NIR) radiation. This is reflected by the objects' surface, and the distance

***Corresponding author: Henrik Lietz,** University of Applied Sciences Ravensburg-Weingarten, Weingarten, Germany,
e-mail: henrik.lietz@hs-weingarten.de
M. Muneeb Hassan and Jörg Eberhardt: University of Applied Sciences Ravensburg-Weingarten, Weingarten, Germany

is determined by calculating the phase difference of both signals [9–12]. Besides the depth information, a PMD sensor generates intensity data using the measurement signal's amplitude information. PMD sensors output a distance image and amplitude image at the same time. Lange describes the PMD's working principle in his dissertation in detail [12]. PMD cameras have to separate their measurement signal from surrounding light for each pixel to reconstruct their modulation frequency. A high amount of extraneous light saturates the pixels and leads to a decrease in accuracy or pixel failures [13]. Reducing the pixel size physically makes it more vulnerable to saturation. To prevent this, the pixel size must be sufficiently large. In outdoor scenarios, it is difficult to reconstruct the inherent modulation signal. First, in the solar spectrum, there is a high amount of IR radiation that saturates the pixels faster than in indoor environments. Second, according to the inverse square law, intensity is inversely proportional to the square of the distance. At large object distances, the measurement signal becomes weaker.

Increasing the sensor's spatial resolution without changing its physical properties is already well-known from 2D imaging [2–6, 14–17]. Computational imaging superimposes an image sequence of degraded LR images via SR algorithms. It addresses reconstruction of high spatial frequencies in continuous object scenes. Therefore, several LR images are sampled in sub-pixel accuracy and registered on a virtual high-resolution sensor grid [3, 4, 15]. At the expense of temporal resolution, computational imaging enhances spatial resolution virtually. Various scientific surveys explain the principle of SR in more detail [2–4, 15].

Current scientific work addresses the resolution enhancement of ToF cameras in different ways. Fusion of two or more range and image acquisition systems [18, 19] expands information density of the object scene. However, this significantly increases the camera's size and cost. Single-frame SR like deconvolution removes optical lens blur [20] by solving a deconvolution problem. This method is strongly limited as no further object information is captured especially for LR sensors when the optical resolving power overcomes the sensor's pixel resolution. Multi-frame SR was adapted to ToF cameras in Refs. [21, 22]. They superimpose several depth images according to Farsiu's fast and robust SR technique [23]. They capture images from slightly displaced viewpoints, by moving the whole camera. This requires large movements of a heavy camera, which seems unsuitable for practical applications. Most of the papers describe spatial resolution enhancement of depth images.

3 Methodology

In this paper, we apply SR on the mobile PMD sensor O3M151 from ifm electronic GmbH, Essen, Germany. Its sensor resolution is of 64×16 PMD pixels, and its immunity to extraneous light reaches up to 120 klx [24]. This makes it suitable for outdoor applications, even in bright daylight. SR reconstruction superimposes a LR image sequence of four LR images according to Köhler's SR algorithm [6], which is implemented in the Multi-Frame Super-Resolution Toolbox (version 1.6.1, Erlangen, Germany) [25]. This SR algorithm overcomes Farsiu's robust SR algorithm [23] for 2D image acquisition as demonstrated in Ref. [6]. As we focus on amplitude images in this paper, we expect a corresponding behavior in the increase in lateral resolution. For the reconstruction process, we assume a point spread function (PSF) with a standard deviation of 0.3 as it provides the best SR results. Image upscaling is set by a factor of two. Motion parameters between successive LR images are known as they are shifted about half a pixel size in horizontal and vertical direction relative to each another. Motorized actuators move a lens transversally to the optical axis, while micrometer screws are used for the sensor-shift method. Each LR image is shifted about ± 0.25 pixels in the horizontal and vertical direction relative to the centered lens position. The LR image sequence encircles the centered lens position. A confined space of $2\ \text{m} \times 4\ \text{m}$ was completely covered in light-absorbing Duvetyne fabric to minimize errors from multi-path interference [26, 27] and ensure constant measuring conditions for all measurements.

4 Super-resolution observation model for low-resolution 3D ToF cameras

Digital imaging can be interpreted as discretizing continuous object scenes. The number of sampling points corresponds to the number of pixels. Although, approximation of continuous object scenes gets better with higher sampling rate, lens aberrations and noise degrade image quality. SR overcomes such limited discretization and degradations by superimposing multiple samples. According to the general observation model [3, 15, 28], one image is captured in full sensor resolution, which represents the ground truth image. It is assumed to be free of aliasing if optical resolving power is below the sensor's Nyquist frequency. Assumption models for motion, blur, down-sampling, and noise degrade and downscale the ground truth image to get a virtually degraded LR sequence. Aliasing occurs after down-sampling the images because optical resolution then exceeds the imager's resolution. SR reconstructs a high-resolution image by inverting that imaging model. SR results are compared with the initial ground truth image [3, 4, 15].

The classical SR observation model is unsuitable for image sensors with low spatial resolution as further down-sampling worsens the quantization. Our proposed SR observation model for LR ToF cameras contains two SR reconstruction branches (see Figure 1), the amplitude image, and the distance image. Optics transfer the continuous object scene on the image sensor and degrades the image by blurring effects, i.e. optical blurring, motion blurring, and sensor blurring. The sensor discretizes the continuous signal corresponding to the sensor resolution and degrades it according to its noise behavior, depicted as additive noise in Figure 1. In order to implement sub-pixel shifts, motion has to be implemented. Motion must be available either in the object or image plane to realize sub-pixel shifts. Based on a sequence of n sub-pixel-shifted LR images, SR algorithms reconstruct high-resolution estimations for both amplitude and distance image separately. SR results are of higher discretization and better quality. However, improvements are limited mostly due to the system's blurring behavior.

5 Measurement setup and evaluation

Generally, SR techniques are evaluated by comparing the SR result with the ground truth image. Quantitative evaluation is then performed by determining the peak signal-to-noise ratio (PSNR) [2, 6, 14]. As we do not have a highly resolved ground truth image, this evaluation method is not feasible. Instead, we determine the system's real optical resolving power by measuring the modulation transfer function (MTF) before and after applying SR. One common method is to use a slanted edge target as proposed in the ISO 12233 standard and described in Ref. [7]. Our measurement procedure is explained in more detail in Ref. [8]. For evaluation, we use Burns' Matlab Toolbox sfrmat3 [29]. Spatial resolution is specified in line pairs per millimeter (LP/mm). Determining spatial frequency response requires a defined target. Two areas of different brightness are separated by a slanted edge. For PMD cameras, contrast transition can be achieved by varying the reflectance in the amplitude image or distance deviation in the distance image. In order to reduce measurement errors, contrast between both partial areas should be more than 20% [30]. This makes it less suitable to apply the slanted edge method on distance images, as a large measurement setup has to be implemented to obtain accurate results. Therefore, we use a flat surface consisting of two regions of different reflectance, realized with black and white cardboards. Both areas are separated by a slanted edge at an angle of 10°. The target's area is 600 mm × 600 mm; measurement distance is 3.5 m. Resolution enhancement is determined from amplitude images only for horizontal direction as the slanted edge is oriented in vertical direction. The result of our lens-shift approach is compared to a common sensor-shift method.

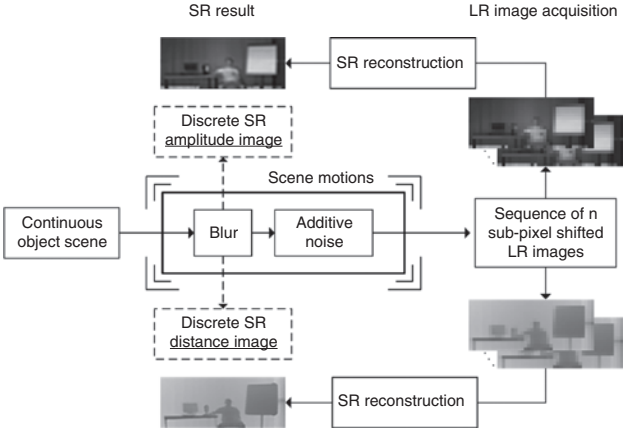

Figure 1: Super-resolution observation model for low-resolution 3D Time-of-Flight sensors. An optical system discretizes continuous object scenes due to a limited number of pixels and degrades it by blurring, noise and motion. Multi-frame super-resolution reconstructs higher spatial frequencies limited by the system's blurring behavior. For ToF cameras, this procedure has to be applied to both, the amplitude and distance images.

Spatial resolution enhancement can be determined on the basis of amplitude data and distance data. The gradient of contrast transition is a measure for the system's lateral resolution. To determine the resolution enhancement in both image types, the target needs varying reflectance as well as distance differences at the same edge. Therefore, we have defined an object scene consisting of four cubes, which differ in size, reflectance, and orientation. SR outputs consist of four LR images, whose sub-pixel shifts were realized according to the lens-shift method. Gradients are determined in both image types at the same position for each LR sample and the SR results. Maximum and minimum intensity values are determined to eliminate outliers. For amplitude images, it is 10% below the highest intensity value and 10% greater than the lowest value. For distance images, these limits are of 5% below or beyond the highest or lowest intensity values. If there is an increase in resolution, contrast transition in the SR result occurs over smaller spatial length, and its gradient is steeper. Resolution enhancement or increase in the slope should be the same for both image types as their pixel size is reduced equally.

6 Opto-mechanical design

To obtain sub-pixel-shifted images, active or passive motion can be used. Active sensor motion via motor actuators needs additional space inside the camera housing. Its advantage is that the travel distance is known, and sub-pixel offset can be predicted precisely. The quality of SR results depends on how well the sub-pixel position is known [17]. For passive motion, like global and local motion in the object scene or vibration and tremors in the sensor's environment, sub-pixel offsets have to be estimated by an additional algorithm. Our suggested lens-shift design provides predictable sub-pixel shifts by transversal movements of an optical lens. There is no need for additional space around the image sensor and further shift-estimating algorithms. Therefore, each type of camera can be extended by SR techniques. Our lens-shift approach significantly increases flexibility, as it does not affect the sensor housing. Furthermore, it can be integrated, even after the camera has been manufactured. In summary, it can be imagined as an inverted optical image stabilization (OIS). As OIS shifts a lens in order to counteract camera movements, we redirect the beam path in a defined manner. This is done to force a beam deflection causing a shift on the image plane similar to moving the sensor. Nevertheless, some properties must be considered. Moving the lens affects aberrations of the optical system. If there is distortion, sub-pixel shifts are not consistent over the entire sensor area. Optical resolving power must overcome the sensor's Nyquist frequency to achieve aliasing, which is important for SR reconstruction [5].

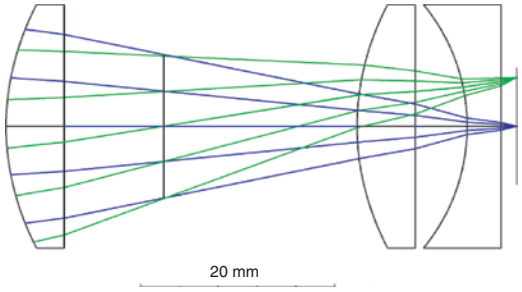

Figure 2: Simulation of the lens-shift design. Our Petzval lens consists of three lenses, two plano-convex aspheres and one plano-concave sphere. First of the three lenses is designed transversely moveable. Blue-coloured beam path represents a field angle of 0°, the green one the maximum horizontal field angle of 6.5°.

For ifm's O3M151 PMD sensor, we have designed a cost-efficient Petzval lens by using stock lenses. It consists of two plano-convex aspheric lenses of 50 mm focal length each and one plano-concave lens of – 25 mm focal length (depicted in Figure 2). The first of the three lenses is transversally movable by motorized actuators Z806 from Thorlabs Inc, Newton, New Jersey, USA. The optical system's focal length is 42.7 mm, the maximum field angle reaches 6.5°, the paraxial magnification is – 0.01246, the entrance pupil diameter is of 20.0 mm, and the wavelength is 850 nm.

Moving the entrance lens has a smaller effect on aberrations than when shifting the other lenses. As the incident light is distributed over almost the complete lens' aperture, small lens shifts do not affect aberrations significantly. Contrarily, when light covers only a small part of the lens' surface, aberration behavior is more sensitive

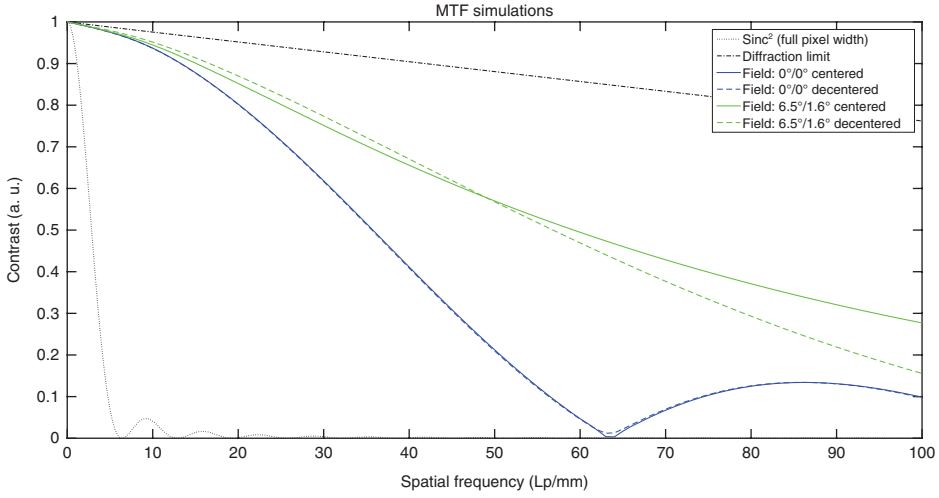

Figure 3: Simulations of the optic's MTF curves compared to the sensor's limiting resolution and the lens' diffraction limit. MTFs for centered and decentered lens positions are simulated for two field angles, 0° and 6.5°/1.6°. Only tangential fields are considered.

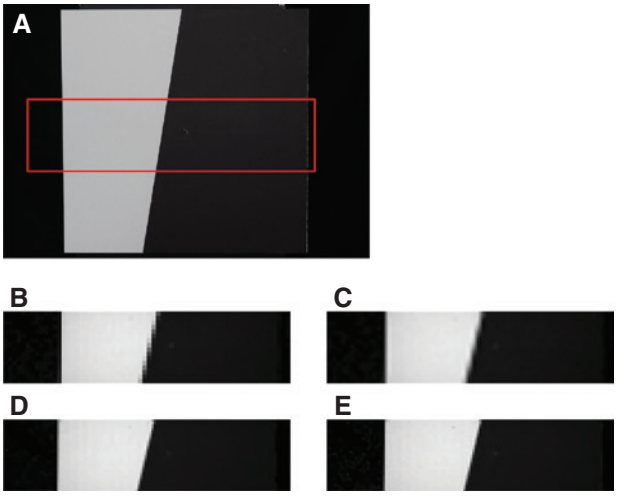

Figure 4: (A) Photo of the slanted edge target, wherein a red box represents the camera's field of view. (B) PMD camera's LR output image, (C) its bicubic interpolation, (D) SR result when shifting the sensor and (E) SR result when shifting the lens.

to lens movements. In addition, the motorized actuator's travel range and resolution are most suited at this position. As mentioned before, optical resolving power must overcome the sensor's limiting resolution. This is proven by our simulations, which are shown in Figure 3. We compare modulation transfer functions (MTFs) for centered and decentered lens positions. Decentered lens position causes a 0.25-pixel offset on the image plane from the centered position. For both positions, MTFs for two borderline cases are shown: one for an incident angle of 0° and another for a maximum incident angle of 6.5° in horizontal and 1.6° in vertical direction. The sensor's theoretical limiting resolution is drawn as a sinc² [31] function for full pixel width. The optical system's theoretical diffraction limit is shown for a wavelength of 850 nm, which is the camera's emitting wavelength. Only tangential fields are considered for simulations of the MTF curves as the target used for our experiments has a vertical edge only.

7 Measurements and results

The first measurement determines resolving power before and after applying SR. Figure 4A shows the original object scene consisting of the slanted edge target. Figure 4B depicts the LR output image and Figure 4C its bicubic interpolation. In Figure 4D and E, the SR results are depicted for conventional sensor-shift method and our lens-shift approach, respectively.

In Figure 4B, a stair step artifact is clearly visible as a result of large pixel dimensions. Its bicubic interpolation in Figure 4C reduces this artifact at the cost of sharpness and results in a blurry image. In both SR results (Figure 4D and E), the stair step artifacts are reduced as sharpness is maintained.

For an objective comparison, MTF curves are shown in Figure 5. The black dotted line represents the sensor's theoretical resolution limit at full pixel width. The initial LR represented by the black solid line shows the real spatial frequency response of the LR image. It can be seen that the initial LR result is close to the theoretical resolution limit. The lines start to diverge at around 4 LP/mm as a result of low quantization. The bicubic interpolation

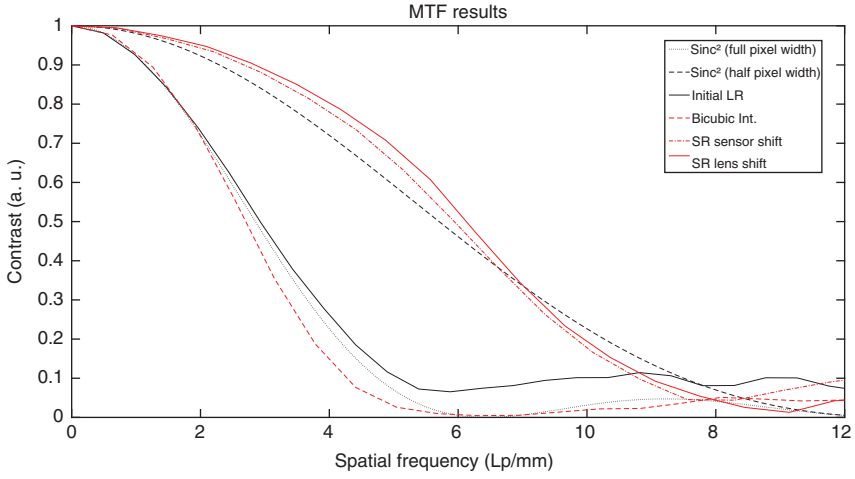

Figure 5: MTF measurement results show spatial frequency responses for various setups. The initial LR camera setup is represented by the black solid line. The red dashed, dash-dotted and solid lines indicate results of bicubic single-frame SR, sensor-shift multi-frame SR and lens-shift multi-frame SR, respectively. The black dotted and dashed lines show the theoretical resolution limit for full pixel and half pixel width.

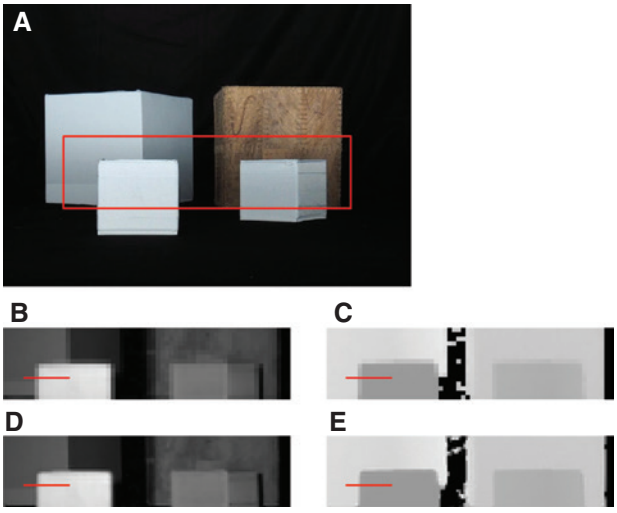

Figure 6: (A) Photo of the measurement scene of four boxes. The red box depicts the camera's field of view. (B) and (C) are the camera's low-resolution (LR) amplitude and distance image outputs. Their associated super-resolution results in (D) and (E) consist of four LR images. Red lines in the camera outputs (B) through (E) mark the position of the corresponding line profiles in Figure 7.

represented by the red dashed line shows worse resolution than the initial LR image. This can also be seen in Figure 4 by comparing Figure 4B and C. This is because missing pixel values are interpolated from real pixel values, and no further object information is acquired. This spreads the contrast transition, which results in a blurry image.

Figure 5 shows significant increase in resolution for the sensor-shift and lens-shift SR. Both solid and dash-dotted red lines are nearly the same. Deviations can be reduced to quantization errors due to the small amount of pixel values. The theoretical resolution limit for half of the initial pixel size is represented as a black dashed line. This overcomes the SR's resolution for higher spatial frequencies as redundant information is acquired during the SR process when shifting the sensor about half a pixel size. This especially affects high spatial frequencies. The SR results resolve spatial frequencies from about 2 LP/mm to 7 LP/mm at higher contrast than theoretically calculated. This can be traced back to computational image restoration, which is part of the SR process. It can be seen that overlapping four LR images is nearly the same as halving the initial pixel size physically.

The second measurement evaluates the resolution enhancement in amplitude and distance image. Figure 6A shows the object scene consisting of four boxes. The red box depicts the camera's field of view. Figure 6B and C represents the LR outputs for the amplitude and distance image, respectively. Their SR results are shown in Figure 6D and E. The red lines in the amplitude and distance images represent the position of the corresponding line profiles in Figure 7.

The resolution of both LR images, amplitude and distance image, is significantly increased after applying our lens-shift method. High spatial frequencies are

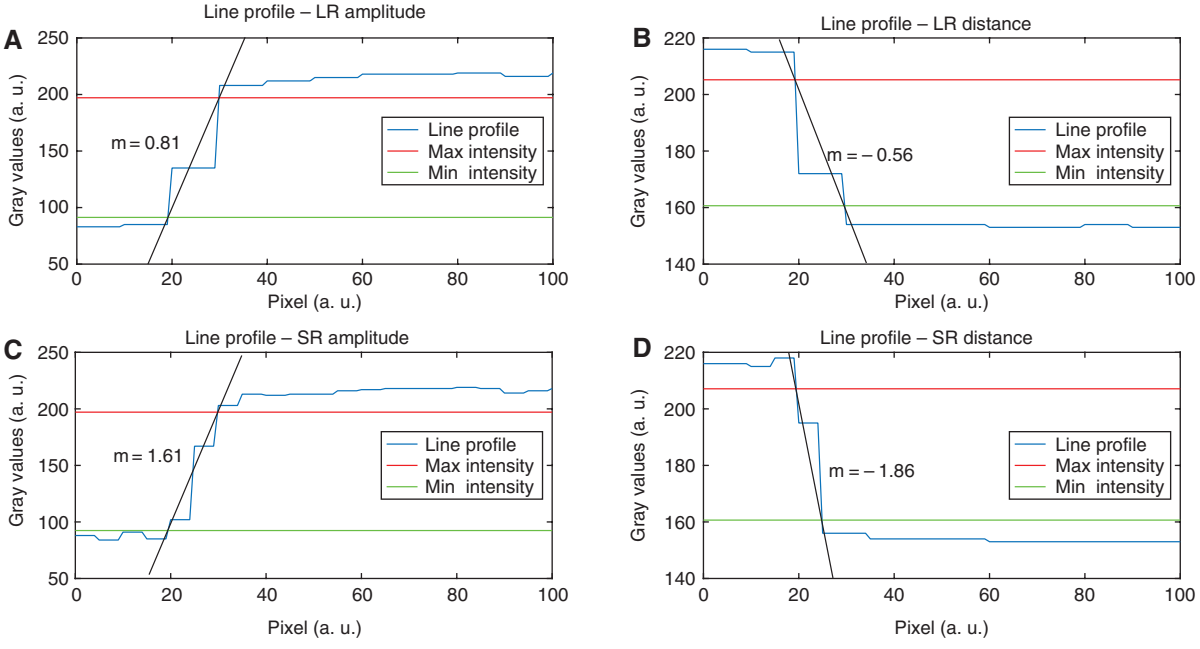

Figure 7: Line profiles of the red lines depicted in Figure 6 (B) through (E). The contrast transition at the edge of the left small cube can be seen in both, amplitude and distance images. Gradient's slope is a measure for the resolving power.

reconstructed, which can be seen especially at the sharpened edges in Figure 6D and E.

The resolution enhancement is determined via the gradient of contrast transition for the LR image and SR result in both image types. Figure 7 shows the line profiles marked as red solid lines in Figures 6B through E.

The gradient in the amplitude image is nearly doubled after applying SR. This confirms our results from the MTF measurements, shown in Figure 5, where resolution is also increased by about a factor of two. Contrary to our expectations, the SR distance image's gradient is more than three times higher than for the initial LR image. This discrepancy is most likely due to the lack of calibration for our lens design. Nonetheless, the resolution enhancement for both image types stays in comparable order of magnitude.

8 Conclusions

In this paper, we described an opto-mechanical lens-shift approach that enables us to record sub-pixel-shifted image sequences without moving the image sensor. It outperforms state-of-the-art sensor-shift approaches in regard to its flexibility as it is even applicable for camera housings that have been manufactured already.

It has been shown that resolution enhancement for the SR result generated by our lens-shift method is close to the theoretical resolution limit if the sensor's pixel size is halved. Future work will focus on further investigation of the discrepancy between resolution enhancement in amplitude and distance images by calibrating the lens.

Acknowledgments: This work has been funded by 'Innovative Projekte 2014'. The authors would like to express their gratitude toward the state of Baden-Württemberg and ifm electronic GmbH for their support during the course of this research.

References

[1] S. Foix, G. Alenya and C. Torras, IEEE Sens. J. 11, 1917–1926 (2011).
[2] J. D. van Ouwerkerk, Image Vision Comput 24, 1039–1052 (2006).
[3] J. Tian and K.-K. Ma, Signal Image Video P. 5, 329–342 (2011).
[4] K. Nasrollahi and T. B. Moeslund, Mach Vision Appl. 25, 1423–1468 (2014).
[5] M. Ben-Ezra, A. Zomet and S. K. Nayar, CVPR 2004, 135–142 (2004).
[6] T. Köhler, X. Huang, F. Schebesch, A. Aichert, A. Maier, et al., IEEE Trans. Comput. Imaging 2, 42–58 (2016).
[7] P. D. Burns and D. Williams, Proc. SPIE 6808, Image Quality and System Performance V 6808 (2008).
[8] H. Lietz and J. Eberhardt, Proc. SPIE 9628, Optical Systems Design 2015: Optical Fabrication, Testing, and Metrology V (9628H) (2015).
[9] R. Lange, P. Seitz, A. Biber and R. Schwarte, Proc. SPIE 3823, Laser Metrology and Inspection (3823) (1999).
[10] R. Lange and P. Seitz, IEEE J. Quantum Elect. 37, 390–397 (2001).
[11] H. G. Heinol, Dissertation (2001).
[12] R. Lange, Dissertation (2000).
[13] T. Möller, H. Kraft, J. Frey, M. Albrecht and R. Lange, Proceedings of the 1st Range Imaging Research Day at ETH, 3-906467 (2005).
[14] T. Köhler, J. Jordan, A. Maier and J. Hornegger, Proceedings of the British Machine Vision Conference (BMVC), 143.1–143.12 (2015).
[15] S. C. Park, M. K. Park and M. G. Kang, IEEE Signal Proc., 20, 21–36 (2003).
[16] Tsai and T. Huang, Advances in Computer Vision and Image Processing, vol. 1, no. 2, JAI Press Inc., 317–339 (1984).
[17] P. Vandewalle, S. Süsstrunk and M. Vetterli, EURASIP J. Adv. Sig. Pr. 2006, 1–15 (2006).
[18] B. Huhle, T. Schairer, P. Jenke and W. Straßer, Comput. Vis. Image Understand. 114, 1336–1345 (2010).
[19] A. Colaco, A. Kirmani, G. A. Howland, J. C. Howell and V. K. Goyal, 2012 IEEE Conference on Computer Vision and Pattern Recognition (CVPR), 96–102 (2012).
[20] L. Xiao, F. Heide, M. O'Toole, A. Kolb, M.B. Hullin, K. Kutulakos, W. Heidrich. 2015 IEEE Conference on Computer Vision and Pattern Recognition (CVPR), 2376–2384 (2015).
[21] S. Schuon, C. Theobalt, J. Davis and S. Thrun, 2009 IEEE Computer Society Conference on Computer Vision and Pattern Recognition Workshops (CVPR Workshops), 343–350 (2009).
[22] S. Schuon, C. Theobalt, J. Davis and S. Thrun, 2008 IEEE Computer Society Conference on Computer Vision and Pattern Recognition Workshops (CVPR Workshops), 1–7 (2008).
[23] S. Farsiu, M. D. Robinson, M. Elad and P. Milanfar, IEEE Trans. Image Process. 13, 1327–1344 (2004).
[24] ifm electronic gmbh, O3M151 data sheet, Available at: http://www.ifm.com/products/de/ds/O3M151.htm, Accessed: 24/Nov/2016.
[25] L. f. Mustererkennung and F.-A.-U. Erlangen-Nürnberg, Multi-Frame Super-Resolution Toolbox, Available at: https://www5.cs.fau.de/research/software/multi-frame-super-resolution-toolbox/, Accessed: 26/Nov/2016.
[26] M. Lindner and A. Kolb, Proc. SPIE 6764, Intelligent Robots and Computer Vision XXV: Algorithms, Techniques, and Active Vision (6764W) (2007).
[27] S. A. Gudmundsson, H. Aanaes and R. Larsen, Environmental Effects on Measurement Uncertainties of Time-of-Flight Cameras, Available at: http://citeseerx.ist.psu.edu/viewdoc/summary?doi=10.1.1.133.4032.
[28] X. Li, Y. Hu, X. Gao, D. Tao, and B. Ning, Signal Process. 90, 405–414 (2010).
[29] sfrmat3: slanted-edge analysis for digital cameras and scanners, Available at: http://losburns.com/imaging/software/SFRedge/index.htm, Accessed: 26/Nov/2016.

[30] P. D. Burns, sfrmat 2.0 User's Guide, Available at: http://read.pudn.com/downloads108/sourcecode/math/448322/sfrmat2_guide.pdf.
[31] G. D. Boreman, Modulation Transfer Function in Optical and Electro-Optical Systems. Bellingham, Washington, USA: SPIE – The International Society for Optical Engineering, 2001.

Henrik Lietz
University of Applied Sciences Ravensburg-Weingarten, Weingarten, Germany
henrik.lietz@hs-weingarten.de

Henrik Lietz studied Optical System Technologies at the University of Applied Sciences Ravensburg-Weingarten and received his MSc degree in 2013. Since then, he has been working as a researcher primarily in the field of 3D camera technology and technical optics. He is currently a PhD student at the Ilmenau University of Technology.

M. Muneeb Hassan
University of Applied Sciences Ravensburg-Weingarten, Weingarten, Germany

M. Muneeb Hassan completed his MSc in Mechatronics from the University of Applied Sciences Ravensburg-Weingarten in 2015. He is currently pursuing his doctorate from the University of Brescia, Italy, and is working as a researcher at the University of Applied Sciences Ravensburg-Weingarten in the field of marker-less motion capture with 3D cameras.

Jörg Eberhardt
University of Applied Sciences Ravensburg-Weingarten, Weingarten, Germany

Jörg Eberhardt studied Information Science majoring in Machine Vision and Machine Learning at the Polytechnic of Konstanz in 1993. After graduating, he carried out further studies and research in the field of 3D scanners and 3D modeling at Coventry University/GB and was awarded a PhD in 1998. From 1999 to 2013, he worked as senior engineer for well-known companies in the field of machine vision where he was responsible for research and development. In 2013, Jörg Eberhardt became an endowed professor for optical technologies at the University of Applied Sciences Weingarten. His research areas are 3D technologies, camera technologies, and machine vision. Jörg Eberhardt is the co-founder of the company Corpus-e, the leading experts in the field of 3D scanning of human body parts.